

Highly stable evolution of Earth’s future orbit despite chaotic behavior of the Solar System

Richard E. Zeebe^{1,*}

**Corresponding Author.*

¹*School of Ocean and Earth Science and Technology, University of Hawaii at Manoa, 1000 Pope Road, MSB 629, Honolulu, HI 96822, USA. email: zeebe@soest.hawaii.edu*

*Accepted, The Astrophysical Journal
January 6, 2022*

ABSTRACT

Due to the chaotic nature of the Solar System, the question of its dynamic long-term stability can only be answered in a statistical sense, for instance, based on numerical ensemble integrations of nearby orbits. Destabilization of the inner planets, including catastrophic encounters and/or collisions involving the Earth, has been suggested to be initiated through a large increase in Mercury’s eccentricity ($e_{\mathcal{M}}$), with an estimated probability of $\sim 1\%$. However, it has recently been shown that the statistics of numerical Solar System integrations are sensitive to the accuracy and type of numerical algorithm. Here I report results from computationally demanding ensemble integrations ($N = 1,600$ with slightly different initial conditions) at unprecedented accuracy based on the full equations of motion of the eight planets and Pluto over 5 Gyr, including contributions from general relativity. The standard symplectic algorithm used for long-term integrations produced spurious results for highly eccentric orbits and during close encounters, which were hence integrated with a suitable Bulirsch-Stoer algorithm, specifically designed for these situations. The present study yields odds for a large increase in Mercury’s eccentricity that are less than previous estimates. Strikingly, in two solutions Mercury continued on highly eccentric orbits (after reaching $e_{\mathcal{M}}$ values > 0.93) for 80-100 Myr before colliding with Venus or the Sun. Most importantly, none of the 1,600 solutions led to a close encounter involving the Earth or a destabilization of Earth’s orbit in the future. I conclude that Earth’s orbit is dynamically highly stable for billions of years in the future, despite the chaotic behavior of the Solar System.

Subject headings: celestial mechanics — methods: numerical — methods: statistical — planets and satellites: dynamical evolution and stability

1. Introduction

One of the oldest and still active research areas in celestial mechanics is the question of the long-term dynamic stability of the Solar System. After centuries of analytical work led by Newton, Lagrange, Laplace, Poincaré, Kolmogorov, Arnold, Moser etc. (Laskar 2013), the field has recently experienced a renaissance due to advances in numerical algorithms and computer speed. Only

since the 1990s have researchers been able to integrate the full equations of motion of the Solar System over time scales approaching its lifetime ($\pm \sim 5$ Gyr) (Wisdom & Holman 1991; Quinn et al. 1991; Sussman & Wisdom 1992; Saha & Tremaine 1992; Murray & Holman 1999; Ito & Tanikawa 2002; Varadi et al. 2003; Batygin & Laughlin 2008; Laskar & Gastineau 2009; Zeebe 2015), and exceeding Earth’s future habitability of perhaps an-

other 1-3 Gyr (Schröder & Smith 2008; Rushby et al. 2013). Looking ahead, detailed exoplanet observations (e.g. Oppenheimer et al. 2013) will enable similar integrations of planetary systems beyond our own solar system.

Importantly, in addition to CPU speed, a statistical approach is necessary due to the chaotic behavior of the Solar System, i.e. the sensitivity of orbital solutions to initial conditions (Laskar 1989; Sussman & Wisdom 1992; Murray & Holman 1999; Richter 2001; Varadi et al. 2003; Batygin & Laughlin 2008; Laskar & Gastineau 2009; Zeebe 2015). To obtain adequate statistics, ensemble integrations are required (Laskar & Gastineau 2009; Zeebe 2015), that is, simultaneous integration of a large number of nearby orbits, e.g. utilizing massive parallel computing. Chaos in the Solar System means small differences in initial conditions grow exponentially, with a time constant (Lyapunov time, e.g. Morbidelli (2002)) for the inner planets of ~ 3 -5 Myr estimated numerically (Laskar 1989; Varadi et al. 2003; Batygin & Laughlin 2008; Zeebe 2015) and ~ 1.4 Myr analytically (Batygin et al. 2015). For example, a difference in initial position of 1 cm grows to ~ 1 AU ($= 1.496 \times 10^{11}$ m) after 90-150 Myr, which makes it fundamentally impossible to predict the evolution of planetary orbits accurately beyond ~ 100 Myr (Laskar 1989). Thus, rather than searching for a single deterministic solution (conclusively describing the Solar System’s future evolution, see Laplace’s demon, Laplace (1951)), the stability question must be answered in probabilistic terms, e.g. by studying the behavior of a large number of physically possible solutions.

Until present, only a single study is available that integrated a large number of Solar System solutions based on the full equations of motion and including contributions from general relativity (Laskar & Gastineau 2009). Using a symplectic integrator throughout, Laskar & Gastineau (2009) integrated 2,501 orbits over 5 Gyr and found that Mercury’s orbit achieved large eccentricities (>0.9) in about 1% of the solutions. Furthermore, they suggested the possibility of a collision between the Earth and Venus. Given that only one study of this kind exists to date, several questions remain. For instance, are the numerical results and statistics obtained sensitive to the numerical algorithm used in the integra-

tions? Furthermore, is the symplectic algorithm used throughout a reliable integrator for highly eccentric orbits and during close encounters? If not, what are the consequences for Solar System stability? In particular, considering long-term stability and planetary habitability, what are the consequences for the evolution of Earth’s future orbit over billions of years? Addressing these questions is the focus of the present study.

2. Methods

I have integrated 1,600 solutions with slightly different initial conditions for Mercury’s position based on the full equations of motion of the eight planets and Pluto over 5 Gyr into the future using the numerical integrator packages **HNBody** (Rauch & Hamilton 2002) and **mercury6** (Chambers 1999). Relativistic corrections (Einstein 1916) are critical (Laskar & Gastineau 2009; Zeebe 2015) and were available in **HNBody** but not in **mercury6**. Post-Newtonian corrections (Soffel 1989; Poisson & Will 2014) were therefore implemented before using **mercury6** (see Appendix). Thus, all simulations presented here include contributions from general relativity (GR). To allow comparison with previous studies, higher-order effects such as asteroids (Ito & Tanikawa 2002; Batygin & Laughlin 2008), perturbations from passing stars, and solar mass loss (Ito & Tanikawa 2002; Batygin & Laughlin 2008; Laskar & Gastineau 2009) were also not included here.

The initial 5-Gyr integrations of the 1,600-member ensemble were performed with **HNBody** (Rauch & Hamilton 2002) using a 4th-order symplectic integrator plus corrector with constant 4-day timestep (Δt , Table 1). The ensemble computations required ~ 6 weeks uninterrupted wall-clock time on a Cray CS300 (~ 1.7 million core hours total), plus up to ~ 4 months for individual runs at reduced timestep (see below). For the symplectic integrations, Jacobi coordinates (Wisdom & Holman 1991) were employed rather than heliocentric coordinates, as the latter may underestimate the odds for destabilization of Mercury’s orbit (Zeebe 2015).

All simulations started from the same set of initial conditions (Table 2), except Mercury’s initial radial distance was offset by 1.75 mm between every two adjacent orbits. The largest overall off-

Table 1: Summary of the 5-Gyr simulations.

$e_{\mathcal{M}}$ ^a	Algorithm ^b	Δt (days)	N	#Collisions ^c	
				$\mathcal{M}\text{-}\mathcal{V}$	$\mathcal{M}\text{-}\mathcal{S}$
< 1.00	4th-sympl.	4	1600		
> 0.55	4th-sympl.	1	28		
$\gtrsim 0.70^d$	4th-sympl.	1/4	10		
$\gtrsim 0.80^e$	BS	adaptive	10	7	3

^a $e_{\mathcal{M}}$ = Mercury’s eccentricity.

^b4th-sympl. = 4-th order symplectic (HNBODY). BS = Bulirsch-Stoer (mercury6).

^c $\mathcal{M}\text{-}\mathcal{V}$: Mercury-Venus, $\mathcal{M}\text{-}\mathcal{S}$: Mercury-Sun.

^dSwitched to 1/4 day-symplectic in case of large $|\Delta E/E|$ variations at 1 day.

^eSwitched to BS in case of $a_{\mathcal{M}}$ shifts and/or large $|\Delta E/E|$ variations at 1/4 day-symplectic.

set was $1,599 \times 1.75 \text{ mm} \simeq 2.80 \text{ m}$, well within the uncertainty of our current knowledge of the Solar System. Initial conditions for all bodies in the 5-Gyr runs (before offsetting Mercury) were generated from DE431 (naif.jpl.nasa.gov/pub/naif/generic_kernels/spk/planets) at JD2451544.5 (01 Jan 2000) using the SPICE toolkit for Matlab (naif.jpl.nasa.gov/naif/toolkit.html) (Table 2). The small offsets in Mercury’s initial position randomized the initial conditions and led to complete divergence of trajectories after $\sim 100 \text{ Myr}$ (see Fig. 4).

In case Mercury’s eccentricity increased above certain threshold values during the simulation (Table 1), Δt was reduced but held constant after that until the next threshold was crossed, if applicable. For example, a 4-fold reduction in stepsize, twice throughout the simulation (i.e. $4 \rightarrow 1 \rightarrow 1/4 \text{ day}$) typically kept the maximum relative error in energy $|\Delta E/E| = |(E(t) - E_0)/E_0|$ and angular momentum ($|\Delta L/L|$) of the symplectic integrator below 10^{-10} and 10^{-11} (Fig. 1). These steps in Δt corresponded to $e_{\mathcal{M}}$ thresholds of about 0.55 and 0.70 (Table 1). All results of the symplectic HNBODY integrations were inspected and (if applicable) restarted manually with smaller Δt at the appropriate integration time using saved coordinates from the run with larger Δt (automatic stepsize reduction was not possible because HNBODY’s source code is not available).

Importantly, high $e_{\mathcal{M}}$ solutions associated with

$a_{\mathcal{M}}$ shifts and/or large $|\Delta E/E|$ variations (usually during close encounters) were integrated using the Bulirsch-Stoer (BS) algorithm with adaptive stepsize control of mercury6, including GR contributions (see Appendix) and specifically designed for these tasks (Chambers 1999) (the symplectic algorithm produced spurious results in these situations, see Figs. 2, 6). Specifically, the symplectic HNBODY integrations (1/4 day) were inspected for $a_{\mathcal{M}}$ shifts and/or large $|\Delta E/E|$ variations and restarted with mercury6’s BS algorithm at the appropriate integration time using saved coordinates from the symplectic HNBODY run. The only comparable study to date (Laskar & Gastineau 2009) integrated 2,501 orbits using a symplectic algorithm and an initial $\Delta t \simeq 9 \text{ days}$. While Laskar & Gastineau (2009) also reduced the timestep depending on $e_{\mathcal{M}}$ (though with generally larger maximum errors, see below), high $e_{\mathcal{M}}$ solutions and close encounters were integrated using the symplectic algorithm throughout (Laskar & Gastineau 2009). However, for highly eccentric orbits the symplectic method can become unstable and may introduce artificial chaos, unless Δt is small enough to always resolve periape (Rauch & Holman 1999). In the Solar System, Δt must hence resolve Mercury’s periape with the highest perihelion velocity (v_p) among the planets (and increasing with e , as $v_p^2 \propto (1+e)/(1-e)$).

3. Results

The vast majority of solutions obtained here showed a stable evolution of the Solar System and moderate $e_{\mathcal{M}}$ values ($e_{\mathcal{M}} < 0.6$ in 99.3% of all runs). In 10 out of 1,600 solutions ($\sim 0.6\%$), Mercury’s eccentricity increased beyond 0.8 (see below). Importantly, the maximum relative error in energy $|\Delta E/E|$ and angular momentum ($|\Delta L/L|$) of the symplectic integrator was typically held below 10^{-10} and 10^{-11} even at $e_{\mathcal{M}} \simeq 0.8$ by e.g. a 4-fold reduction in stepsize twice throughout the simulation (Fig. 1). Critically, once $e_{\mathcal{M}}$ increased beyond ~ 0.8 (resulting in close encounters with Venus and shifts in Mercury’s semi-major axis, $a_{\mathcal{M}}$), the Bulirsch-Stoer integrator of mercury6 was employed. For example, in run #0299 (R0299 for short) close encounters between Mercury and Venus occurred at $t \simeq 4.3042 \text{ Gyr}$ at which time they approach their mutual Hill radius (Chambers

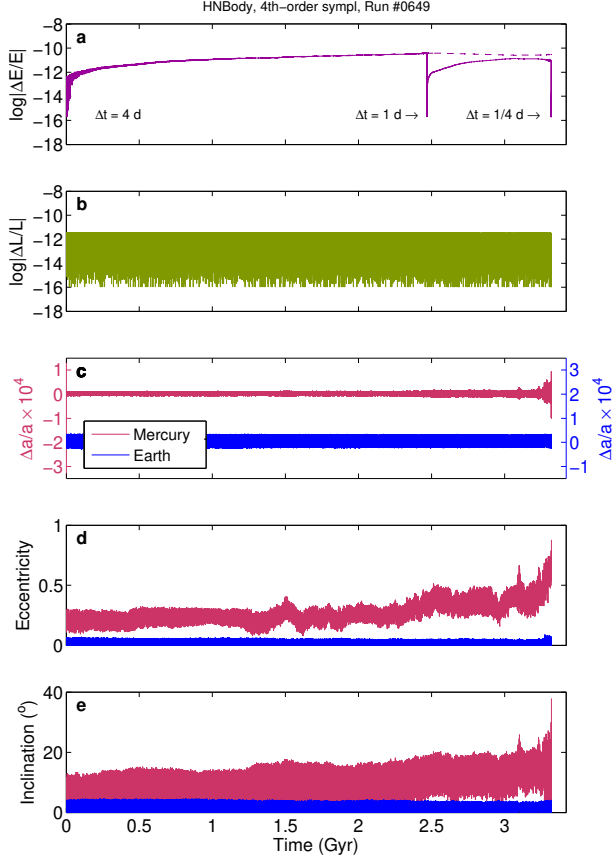


Fig. 1.— Example of a symplectic multi-billion year integration of the Solar System with HNBODY (run #0649). Results shown are from symplectic integrator only (4-th order with corrector and Jacobi coordinates), not from Bulirsch-Stoer integrator (see text). (a) Relative energy error, $|\Delta E/E| = |(E(t) - E_0)/E_0|$. After the two reductions in integrator timestep (t_i , $i = 1, 2$), solid and dashed lines show $|\Delta E/E|$ relative to $E(t_i)$ and relative to absolute $E_0(t_0 = 0)$, respectively. (b) Relative angular momentum error, $|\Delta L/L| = |(L(t) - L_0)/L_0|$. (c) Change in Mercury’s and Earth’s semi-major axes, $\Delta a/a = (a(t) - a_0)/a_0$. (d) Mercury’s and Earth’s eccentricity (e_M , e_E). (e) Inclination. Note that $|\Delta E/E| < 10^{-10}$, even at $e_M \simeq 0.8$. When oscillations in $|\Delta E/E|$ and/or shifts in a_M occurred ($e_M \gtrsim 0.8$), integrations were continued with `mercury6`’s Bulirsch-Stoer algorithm (see Figs. 2, 5, 6).

et al. 1996):

$$r_H = \frac{a_M + a_V}{2} \left(\frac{m_M + m_V}{3m_1} \right)^{1/3} \simeq 0.0053 \text{ AU}, \quad (1)$$

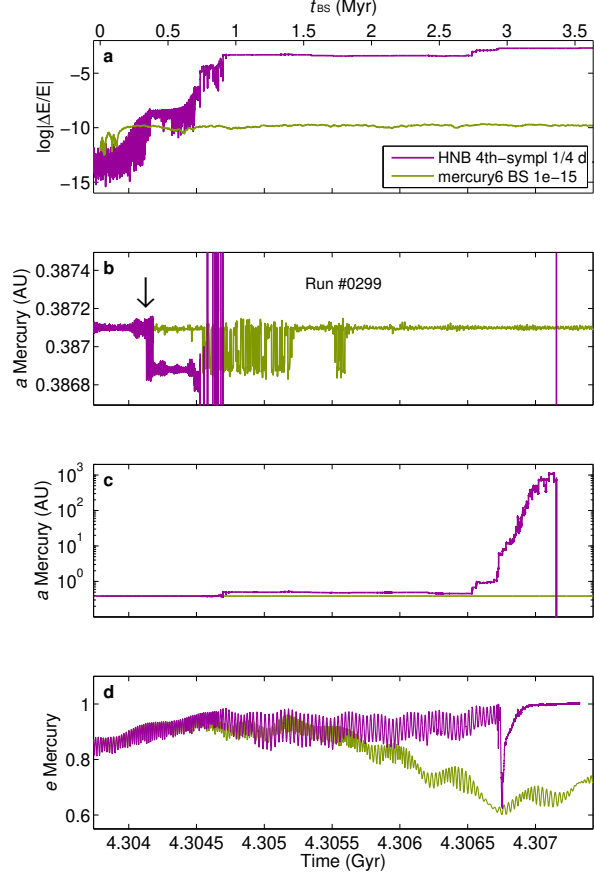


Fig. 2.— Symplectic and Bulirsch-Stoer (BS) integration of run #0299 at high e_M . The BS integration (`mercury6`, green lines, approximate relative x and v error per step = 10^{-15}) was initiated at $t_{BS} = 0$ using the coordinates of the symplectic run (HNB = HNBODY, purple lines, 4-th order, timestep = 1/4 day). (a) Relative energy error, $|\Delta E/E|$. (b) and (c) Mercury’s semi-major axis, a_M (note different y-scales). (d) Mercury’s eccentricity, e_M . Note spurious drop in a_M at $t_{BS} \simeq 340$ kyr in the symplectic integration (arrow), which ultimately causes rapid destabilization of Mercury’s orbit (see text). In contrast, a_M is essentially stable in the BS integration, which properly resolves Mercury’s periaapse and close encounters as a result of adaptive step size control.

where a ’s and m ’s are the planetary semi-major axes and masses; m_1 is the solar mass.

More precisely, close encounters with $d_{min} = 0.0080$ AU ensued at $t_{BS} \simeq 340$ kyr, where t_{BS} is measured from the start of the BS integration

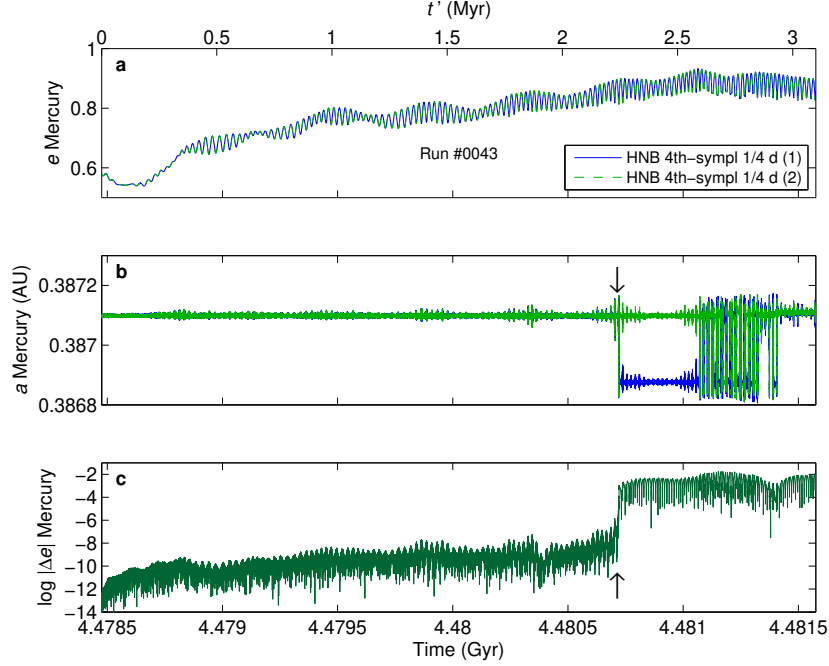


Fig. 3.— Illustration of trajectory separation as Mercury’s orbit approaches instability. (a) $e_{\mathcal{M}}$ from two symplectic integrations with HNBODY of Run 0043 of one fiducial (solid blue line, Nr. (1)) and one shadow orbit (dashed green line, Nr. (2)) offset by 1.75 mm in Mercury’s x -coordinate at $t' = 0$. (b) Mercury’s semi-major axis. (c) Difference in $e_{\mathcal{M}}$ ($\Delta e_{\mathcal{M}}$) between (1) and (2). At $t' \simeq 2.2$ Myr, close encounters between Mercury and Venus ensue (see jumps in $a_{\mathcal{M}}$ and $\Delta e_{\mathcal{M}}$, arrows).

and d_{min} is the minimum distance between the two bodies (Fig. 2). This point in time corresponds to a significant drop of $a_{\mathcal{M}}$ to ~ 0.3869 AU in the symplectic integration, while $a_{\mathcal{M}}$ in the BS integration remains stable. Note that the corresponding symplectic $|\Delta E/E| < 10^{-8}$ at 340 kyr may be misinterpreted to reflect accurate orbit integration (in fact, if the symplectic Δt was reduced right afterwards, spurious behavior would likely go unnoticed). However, this is clearly not the case as shown by comparison with BS, which, due to adaptive step size control, properly resolves Mercury’s periape and close encounters. Hence the relative energy error (say $\lesssim 10^{-8}$, Laskar & Gastineau (2009)) is not a sufficient criterion to ensure accurate steps in symplectic integrations with highly eccentric orbits and close encounters.

The drop in $a_{\mathcal{M}}$ at $t_{BS} \simeq 340$ kyr in the symplectic R0299 integration preconditions the system for further $e_{\mathcal{M}}$ increase, subsequently causing a large $a_{\mathcal{M}}$ rise and rapid destabilization of Mercury’s orbit (Fig. 2). Specifically, the $a_{\mathcal{M}}$ drop is followed by an immediate increase in the average $e_{\mathcal{M}}$ in the symplectic integration relative to BS, which, in turn degrades Mercury’s perihelion resolution (at constant symplectic Δt) and leads to oscillations in $|\Delta E/E|$ and to further, larger swings in $a_{\mathcal{M}}$. In contrast, while in the BS integration $a_{\mathcal{M}}$ also oscillates, it remains overall fairly stable over several million years. Eventually, Mercury collides with Venus in BS-R0299 at $t_{BS} \simeq 15$ Myr (Fig. 5). Thus, while ultimately both the symplectic and BS integration of R0299 spell disaster for Mercury’s orbit, it involves vastly different trajectories and time scales. Notably, Mercury’s extended lifetime in the BS integration relative to the symplectic algorithm is a common feature (see Figs. 5, 6). One reason for this is of course a too large (and constant) timestep in the current symplectic integrations. The crux, however, is that even if the symplectic timestep was reduced before $|\Delta E/E|$ becomes too large, spurious results could easily be overlooked.

Note that the spurious $a_{\mathcal{M}}$ shift in the symplectic integration of R0299 occurs after only a

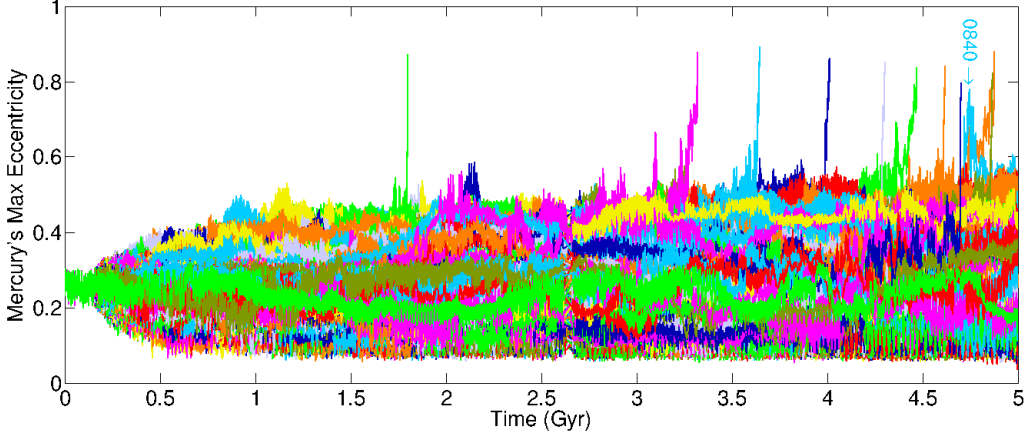


Fig. 4.— Mercury’s maximum eccentricity per 1 Myr bin from the 1,600 symplectic 5-Gyr integrations. Results shown are from `HNBody`’s symplectic integrator only (Rauch & Hamilton 2002). In ten solutions, $e_{\mathcal{M}}$ crossed 0.8, after which the integration was continued with `mercury6`’s Bulirsch-Stoer algorithm (Chambers 1999) (Fig. 5). Note that in R0840 (arrow), $e_{\mathcal{M}} < 0.8$, no shifts in $a_{\mathcal{M}}$ occurred, and $\max |\Delta E/E| \simeq 8 \times 10^{-11}$.

few 100 kyr during close encounters ($t_{BS} = 0$ means same coordinates in symplectic and BS integration) and is therefore not due to intrinsic chaos, whose characteristic time scale causes trajectory separation over millions of years. The million-year separation time still holds even as Mercury’s orbit approaches the regime of instability in the solutions studied here ($e_{\mathcal{M}} \gtrsim 0.8$). This behavior can be illustrated by following two nearby trajectories initiated at high $e_{\mathcal{M}}$ (Fig. 3). One fiducial and one shadow orbit of R0043 offset by 1.75 mm in Mercury’s x -coordinate were integrated using `HNBody`’s symplectic algorithm. Polynomial growth in $\Delta e_{\mathcal{M}}$ (difference in $e_{\mathcal{M}}$ between the two orbits) governs $\Delta e_{\mathcal{M}}$ ’s increase over the first ~ 2.2 Myr (cf. Zeebe 2015). However, at $t' \simeq 2.2$ Myr, close encounters between Mercury and Venus ensue (as in R0299), causing jumps in $a_{\mathcal{M}}$ and $\Delta e_{\mathcal{M}}$ (arrows, Fig. 3). Additional shadow runs initiated at $t' = -26$ Myr and -11 Myr (not shown) exhibit no close encounters during run-up to $t' = 2.2$ Myr and indicate exponential trajectory divergence due to chaos after $\gtrsim 8$ Myr. Thus, the abrupt divergence of trajectories at 2.2 Myr is due to close encounters, not intrinsic chaos.

3.1. High- $e_{\mathcal{M}}$ solutions

In ten solutions, $e_{\mathcal{M}}$ increased beyond 0.8 of which seven (three) resulted in collisions Mercury-Venus (Mercury-Sun) (Table 1, Fig. 4). Thus, the odds for a large increase in Mercury’s eccentricity found here (0.6%) are less than previous estimates of $\sim 1\%$ (Laskar & Gastineau 2009). Strictly, the latter odds were actually $20/2501 = 0.8\%$. Using different statistical methods (e.g. Agresti & Coull 1998), the 95% confidence interval for the two results (0.6% and 0.8%) may be estimated as $\pm 0.42\%$ ($N = 1,600$) and $\pm 0.36\%$ ($N = 2,501$). Thus at the 95% confidence level, one can conclude that the two results are not statistically different from one another, which could be remedied by performing ensemble runs with even larger N . It is important to realize, however, that in order to reduce the 95% confidence interval for the same distributions to, say $\pm 0.1\%$ would require $N \gtrsim 20,000$. Note that the 1,600 solutions used initial conditions that differed only by 1.75 mm in Mercury’s initial radial distance between every two adjacent orbits. Yet the small offsets in Mercury’s initial position randomized the initial conditions and led to complete divergence of trajectories after ~ 100 Myr (Fig. 4).

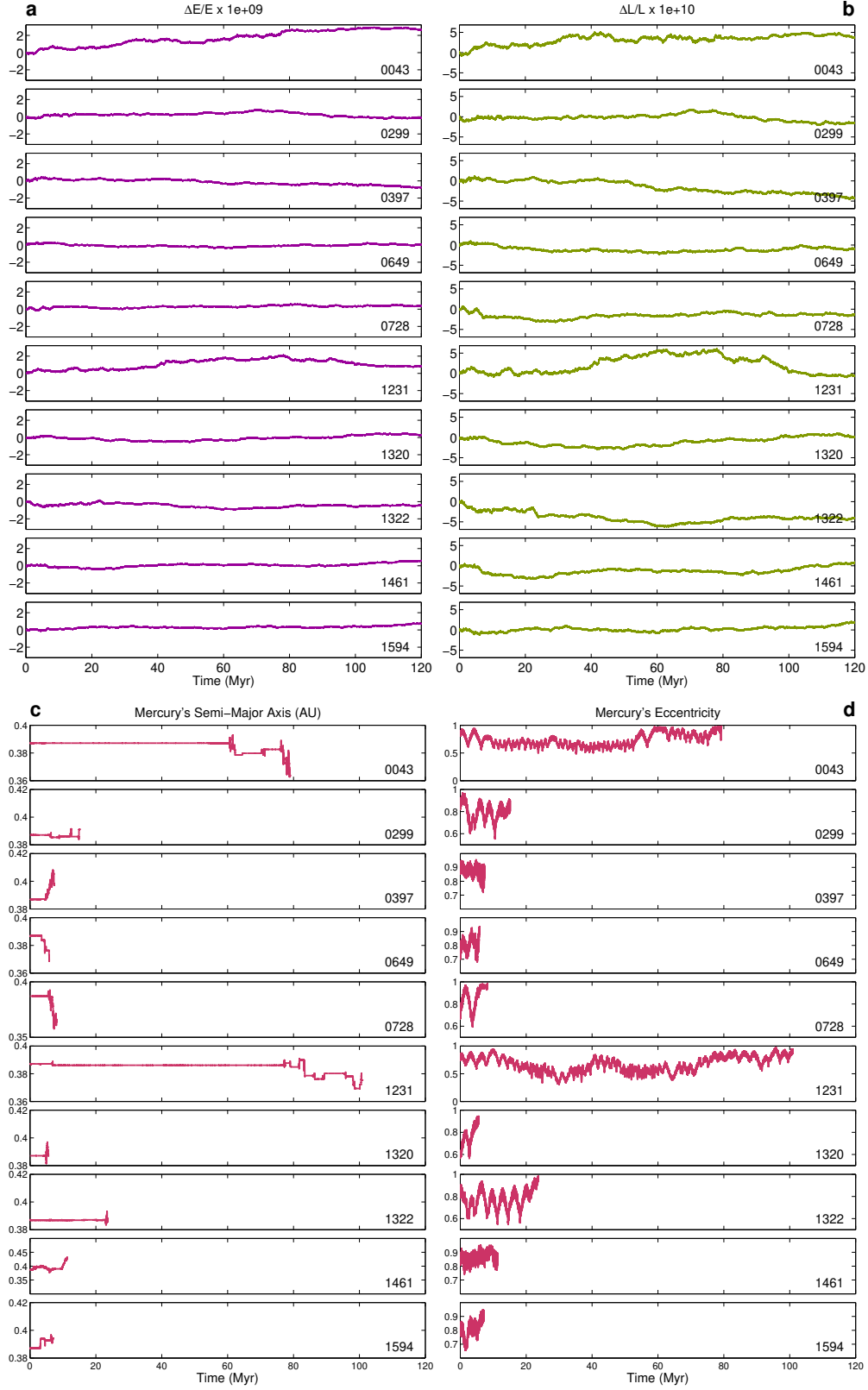


Fig. 5.— 120 Myr of Bulirsch-Stoer integration of ten solutions, initiated when oscillations in $|\Delta E/E|$ and/or shifts in a_M occurred in the symplectic integrations ($e_M \gtrsim 0.8$, see text). (a) Relative error in energy and (b) angular momentum. (c) Mercury's semi-major axis and (d) eccentricity. Note solutions R0043 and R1231.

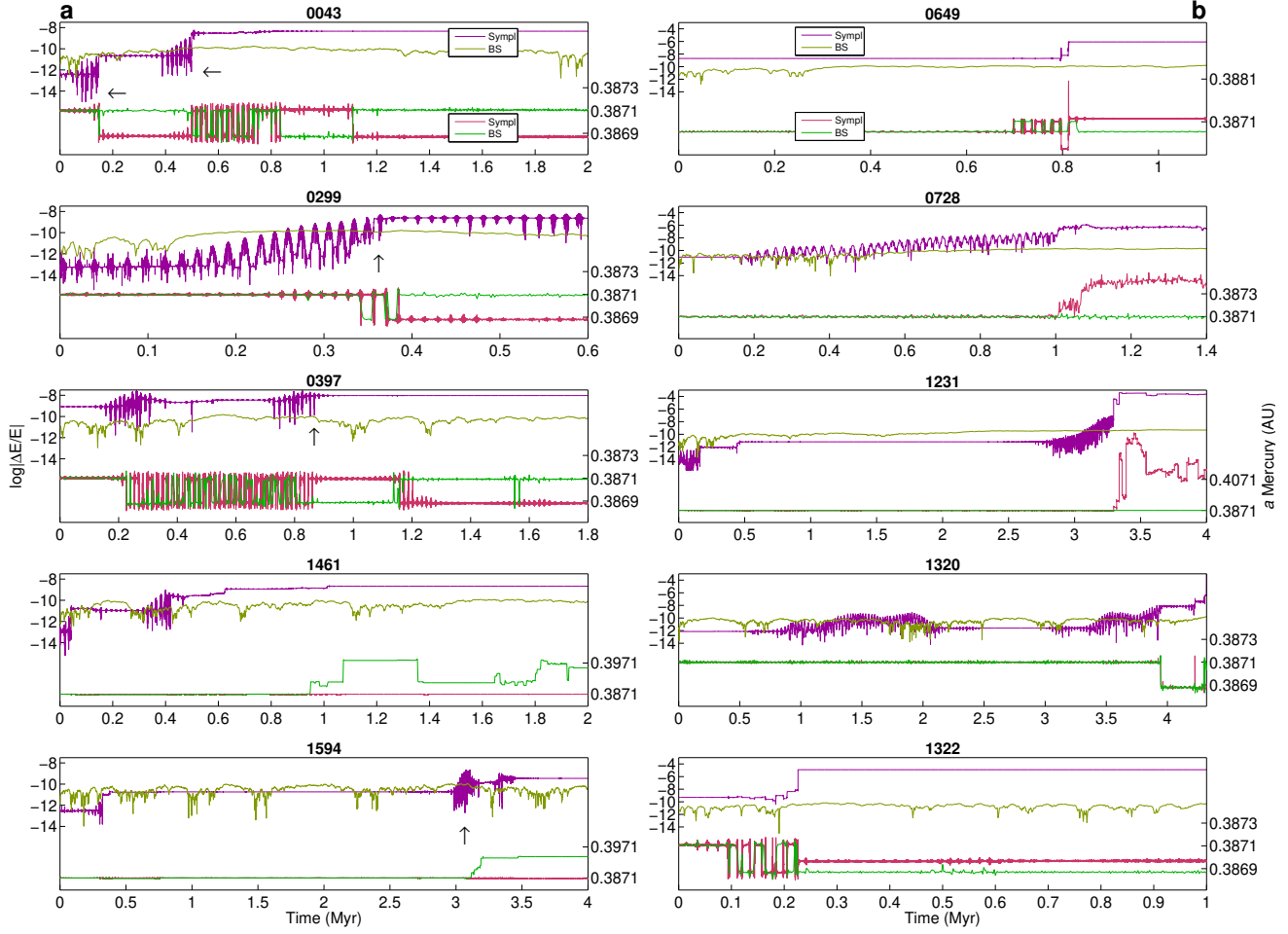


Fig. 6.— Comparison of symplectic vs. BS integration of all ten high- $e_{\mathcal{M}}$ solutions during the initial phase (cf. Fig. 2). In each panel, the top two graphs show $\log|\Delta E/E|$ (left axes), the bottom two graphs show $a_{\mathcal{M}}$ (right axes). (a) Column of five runs with ‘initial’ symplectic $|\Delta E/E| \lesssim 10^{-8}$ (see text). Note symplectic $|\Delta E/E|$ oscillations $< 10^{-8}$ (arrows, corresponding to high $e_{\mathcal{M}}$ periods) after which symplectic and BS trajectories diverge (indicated by different subsequent $a_{\mathcal{M}}$ evolutions). (b) Five runs with ‘initial’ symplectic $|\Delta E/E| > 10^{-8}$ (see text).

The results of the symplectic algorithm were used only until shifts in $a_{\mathcal{M}}$ and/or large $|\Delta E/E|$ variations occurred in the 1/4 day-symplectic integration ($e_{\mathcal{M}} > 0.8$, Fig. 4). Subsequently, the integration was continued with `mercury6`'s Bulirsch-Stoer (BS) algorithm (Fig. 5) (all integrations included GR contributions, see Appendix). As is well known, long-term conservation of energy and angular momentum in BS integrations (here: $|\Delta E/E| \lesssim 2 \times 10^{-9}$, $|\Delta L/L| \lesssim 5 \times 10^{-10}$) is generally worse than in symplectic integrations. However, as mentioned above, for highly eccentric orbits the symplectic method can become unstable and may introduce artificial chaos (Rauch & Holman 1999). Thus, in the present case (critical time interval $\lesssim 100$ Myr), it was imperative to integrate high $e_{\mathcal{M}}$ solutions and close encounters with `mercury6`'s BS algorithm (adaptive stepsize control), specifically designed for these tasks (Chambers 1999). The symplectic algorithm produced spurious results in these situations (Figs. 2, 6).

All ten solutions with $e_{\mathcal{M}} > 0.8$ integrated with Bulirsch-Stoer ultimately resulted in collisions involving Mercury; Mercury-Venus: R0299, R0397, R0649, R1231, R1320, R1461, and R1594; Mercury-Sun: R0043, R0728, and R1322. Strikingly, in two solutions (R0043 and R1231), Mercury continued on highly eccentric orbits (after reaching $e_{\mathcal{M}}$ values > 0.93) for 80-100 Myr before colliding with Venus or the Sun (Fig. 5). This suggests the potential existence of non-catastrophic trajectories, despite Mercury achieving large eccentricities (is there a chance of recovery, evading detrimental consequences for the Solar System?). In contrast, once $e_{\mathcal{M}}$ crossed 0.90-0.95 in the symplectic integrations ($\Delta t = 1/4$ day), large shifts in $a_{\mathcal{M}}$ and/or energy occurred rapidly, often leading to complete destabilization of Mercury's orbit within less than a few million years (Figs. 2, 6). Once Mercury was removed (merged with Venus/Sun via inelastic collision), the system behaved very stable (no indication of chaotic behavior in the BS integrations).

3.2. High- $e_{\mathcal{M}}$ solutions: Symplectic vs. Bulirsch-Stoer results

As mentioned above, the symplectic integrations of the ten high- $e_{\mathcal{M}}$ solutions (smallest $\Delta t = 1/4$ day) quickly failed once $e_{\mathcal{M}}$ reached 0.90-0.95. In five out of ten runs, the deterioration of the inte-

grations was immediately obvious because the relative energy error, $|\Delta E/E|$, rapidly grew beyond 10^{-8} due to the constant 1/4-day timestep, which was clearly too large for these runs (Fig. 6). However, the symplectic $|\Delta E/E|$ remained 'initially' below $\sim 10^{-8}$ in the other five runs, which, if focusing only on the maximum energy error, may not raise a red flag. Yet, large oscillations and jumps in the symplectic $|\Delta E/E|$ occurred in these five runs during high- $e_{\mathcal{M}}$ periods, after which the symplectic trajectories rapidly diverged from the BS trajectories (Fig. 6). ('Initially' here refers to the time interval when $|\Delta E/E| < 10^{-8}$ but trajectories already diverge; if symplectic Δt is reduced subsequently, spurious behavior may go unnoticed). Note that while $|\Delta E/E|$ was still $< 10^{-8}$ after these events, $|\Delta E/E|$ in the symplectic integrations was typically two orders of magnitude larger than in the BS integrations at that point. In runs 0043, 0299, and 0397, $a_{\mathcal{M}}$ values in the symplectic integrations subsequently dropped below those of the BS runs. In runs 1461 and 1594, $a_{\mathcal{M}}$ shifted to larger values in the BS integrations, which are missed in the symplectic integrations. These observations reiterate the point made above that even though the symplectic relative energy error may remain below a certain threshold (say $< 10^{-8}$), this does not guarantee accurate orbit integration, for instance, during close encounters and for highly eccentric orbits.

Ultimately, eight of the ten symplectic high- $e_{\mathcal{M}}$ integrations resulted in large oscillations and jumps in $|\Delta E/E|$ to values $> 10^{-8}$. In addition, runs 0043, 0299, and 0728 resulted in rapid destabilization of Mercury's orbit ($e_{\mathcal{M}} > 0.99$ and large shifts in $a_{\mathcal{M}}$). Two runs (1461 and 1594) conserved $|\Delta E/E|$ values to below 10^{-8} but featured a rapid, suspicious decline in $e_{\mathcal{M}}$ and missed the $a_{\mathcal{M}}$ shifts seen in the BS runs (see above). Thus all ten symplectic high- $e_{\mathcal{M}}$ integrations essentially failed within only ~ 4 Myr once $e_{\mathcal{M}}$ had reached critical values between 0.90 and 0.95. The short lifetime of the highly eccentric Mercurian orbits in the symplectic integrations (compared to the much longer lifetime in the BS integrations, see Fig. 5) is of course mostly a result of too large a timestep, which was constant throughout the symplectic integration. However, the critical point is that even if the symplectic timestep was reduced during the integration to maintain a certain energy

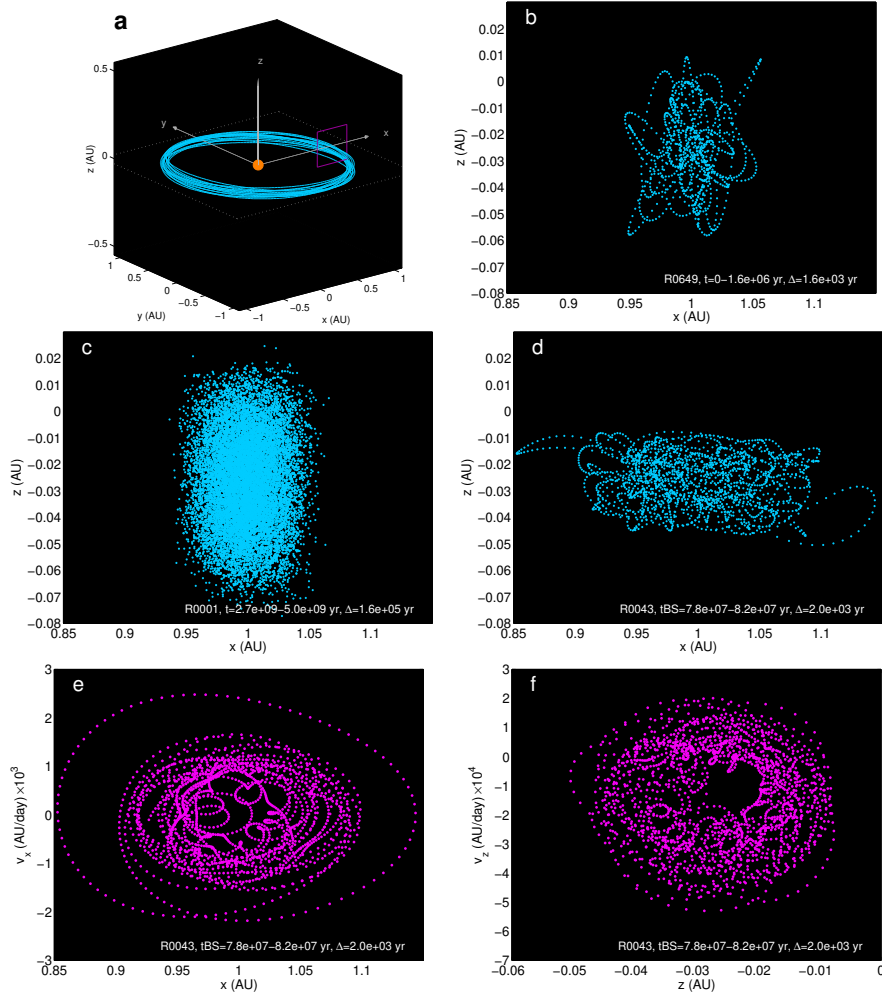


Fig. 7.— Illustration of the stability of Earth’s orbit. (a) Earth’s orbital path in the heliocentric Cartesian system (shown are 15 orbits of R0001, separated by 100 kyr each). The area of intercept of Earth’s trajectory with the xz -plane ($x > 0$) is indicated by the purple rectangle (size not to scale). (b) Dots represent the intercepts during the first 1.6 Myr of R0649 plotted every 1,600 yr. (c) Intercepts during the final 2.3 Gyr of R0001 plotted every 160 kyr. (d) Intercepts during a 4-Myr period of R0043 plotted every 2,000 yr. The minimum and maximum x -values (~ 0.85 and ~ 1.15 AU) occur during a ~ 200 kyr interval just before Mercury collides with Venus. (e) Poincaré section of Earth’s trajectory in phase space: x -velocity vs. x -coordinate when Earth’s trajectory crosses the xz -plane ($x > 0$), corresponding to (d). (f) Same as (e) but z -velocity vs. z -coordinate. Note that in all 1,600 solutions integrated here, Earth’s orbital path intersected the xz -plane within an area bounded by x and z -coordinates that varied at most by ± 0.15 and ± 0.05 AU from the mean. The corresponding x and z -velocities varied at most by $\pm 2.5 \times 10^{-3}$ and $\pm 9.0 \times 10^{-4}$ AU day $^{-1}$ from the mean.

error (Δt can not be changed too often though), symplectic integrators can easily produce spurious results for highly eccentric orbits and during close encounters, as demonstrated by the comparison with the BS integrations.

3.3. Future evolution of Earth’s orbit

Mercury’s orbital dynamics had little effect on Earth’s orbit as none of the 1,600 solutions showed a destabilization of Earth’s future orbit over the next 5 Gyr. Rather, Earth’s future orbit was highly stable. For illustration, during a typical, full 5-Gyr run, Earth’s orbital path typically intersected the xz -plane of the heliocentric Carte-

sian system within an area bounded by x and z -coordinates that varied at most by ± 0.07 and ± 0.05 AU from the mean, respectively (Fig. 3.2). In the most extreme case found here (R0043), x and z varied at maximum by ± 0.15 and ± 0.05 AU (Earth’s eccentricity approaching 0.15). Importantly, the maximum x, z variations in R0043 were actually restricted to a ~ 200 kyr interval just before Mercury collided with Venus (Fig. 3.2). Poincaré sections of Earth’s trajectory in phase space showed that the corresponding x and z -velocities in all 1,600 solutions varied at most by $\pm 2.5 \times 10^{-3}$ and $\pm 9.0 \times 10^{-4}$ AU day $^{-1}$ from the mean (Fig. 3.2).

Also, none of the 1,600 simulations led to a close encounter, let alone a collision, involving the Earth. The minimum distance between the Earth and another planet (viz. Venus, $d_{min} \simeq 0.09$ AU) occurred in R0728 during a 50-year period when Mercury collided with the Sun. This d_{min} does not qualify as a close encounter though; it is still ~ 9 times larger than the Earth-Venus mutual Hill radius, $r_H \simeq 0.01$ AU (Chambers et al. 1996), or $\sim 1/3$ of the current d_{min} ($\sim 30 \times r_H$). A previous study suggested the possibility of a collision between the Earth and Venus via transfer of angular momentum from the giant planets to the terrestrial planets (Laskar & Gastineau 2009). However, the total destabilization of the inner Solar System only occurred after e_M had already crossed 0.9 and $|\Delta E/E|$ had grown beyond 2×10^{-8} in their symplectic integration (Laskar & Gastineau 2009). Did such disastrous trajectories for the Earth arise because Mercury’s periape and close encounters were not adequately resolved at some point in the symplectic integration?

The values of Earth’s orbital elements semi-major axis (a_E), eccentricity (e_E), and inclination (i_E) remained within narrow bands in all 1,600 solutions studied here (Fig. 8). For instance, $\max(a_E) < 1.0005$ AU, $\max(e_E) < 0.15$, and $\max(i_E) < 5.1$ deg (for comparison, J2000 mean values are $a_E = 1.0000$, $e_E = 0.017$, $i_E = 0.0$ deg). As the present study essentially sampled eight trillion annual realizations of possible Solar System configurations in the future ($1,600 \times 5 \cdot 10^9$), the near constancy of Earth’s orbital elements a, e and i suggests that Earth’s orbit is dynamically highly stable for billions of years to come.

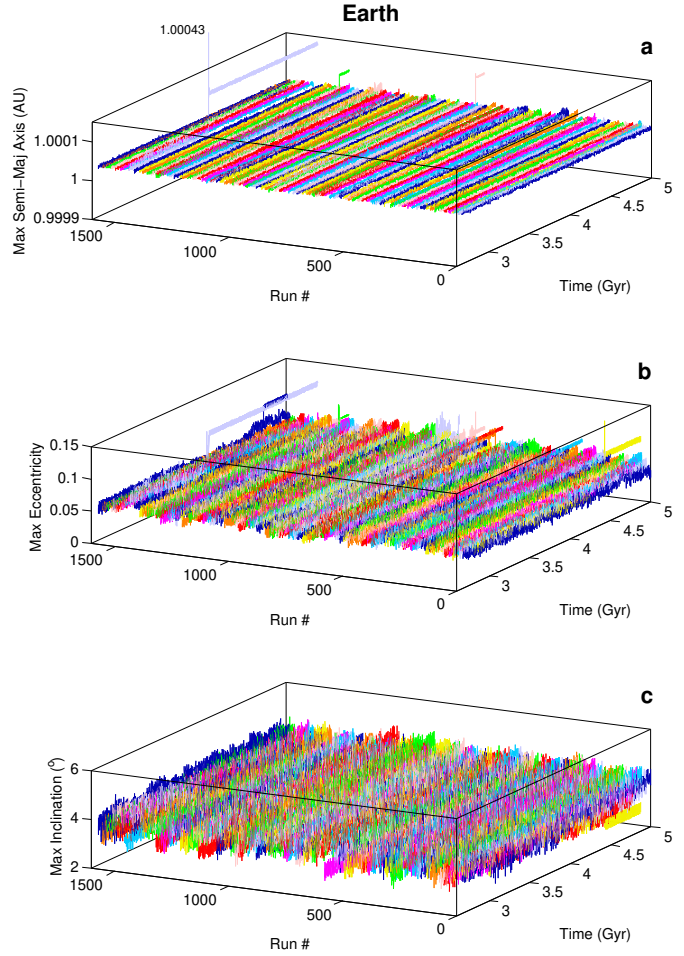


Fig. 8.— Maximum values per 1-Myr bin of Earth’s slowly changing orbital elements. (On gyr-time scale, argument of periaapsis, longitude of ascending node, and mean anomaly may be considered ‘fast angles’.) For better visualization, only every 20th of the 1,600 solutions are plotted plus all runs with $e_M > 0.8$ for $t = 2.5$ – 5 Gyr. The 1,600 solutions used initial conditions that differed only by 1.75 mm in Mercury’s initial radial distance between every two adjacent orbits. (a) Maximum semi-major axis, (b) eccentricity, and (c) inclination. All three elements remained within narrow bands in the 1,600 solutions: $\max(a_E) < 1.0005$ AU, $\max(e_E) < 0.15$, and $\max(i_E) < 5.1$ deg. The runs with elevated a_E and e_E are solutions with large increases in Mercury’s eccentricity. For example, a_E reached 1.00043 AU in R1461 during a high- e_M interval, which occurred ~ 8 Myr before Mercury collided with Venus. After Mercury had been merged with Venus, the system behaved very stable.

4. Conclusions

In the present manuscript, I have reported results from computationally demanding ensemble integrations ($N = 1,600$) of the Solar System's full equations of motion at unprecedented accuracy over 5 Gyr. All integrations included relativistic corrections, which substantially reduce the probability for Mercury's orbit to achieve large eccentricities. The computations show that the relative energy error in symplectic integrations (say $\lesssim 10^{-8}$) is not a sufficient criterion to ensure accurate steps for highly eccentric orbits and during close encounters. The calculated odds for a large increase in Mercury's eccentricity are less than previously estimated. Most importantly, none of the 1,600 solutions led to a close encounter, let alone a collision, involving the Earth. I conclude that Earth's orbit is dynamically highly stable for billions of years in the future, despite the chaotic behavior of the Solar System. A dynamic lifetime of $\gtrsim 5$ Gyr into the future may be somewhat short of the Sun's red giant phase when most inner planets will likely be engulfed, but clearly exceeds Earth's estimated future habitability of perhaps another 1-3 Gyr (Schröder & Smith 2008; Rushby et al. 2013).

Acknowledgments. This project would not have been possible without the HPC cluster test-phase of the University of Hawaii. I thank Ron Merrill, Sean Cleveland, and Gwen Jacobs for providing the opportunity to participate in the test program. The anonymous reviewer is thanked for valuable comments, which improved the manuscript. I am grateful to Peter H. Richter who dared to introduce us to Chaos, Poincaré, and Solar System dynamics in a 1989-undergraduate physics course on classical mechanics. Nemanja Komar's assistance in analyzing the numerical output was greatly appreciated.

A. Contributions from general relativity

Relativistic corrections (Einstein 1916) are critical as they substantially reduce the probability for Mercury's orbit to achieve large eccentricities (Laskar & Gastineau 2009; Zeebe 2015). General relativity (GR) corrections are available in `HNBody` but not in `mercury6`. First Post-Newtonian (1PN) corrections (Soffel 1989; Poisson & Will 2014) were therefore implemented before using `mercury6`'s Bulirsch-Stoer algorithm.

Because of the Sun's dominant mass, GR effects are considered only between each planet and the Sun, not between planets. Relative to the barycenter, the 1PN acceleration (denoted by $\tilde{}$) due to the Sun's mass m_1 on planet $j = 2, N$ may be written as (Soffel 1989; Poisson & Will 2014):

$$\begin{aligned} \tilde{\mathbf{a}}_j = & \frac{1}{c^2} \left\{ \frac{Gm_1}{r_j^3} \left[-v_j^2 - 2v_1^2 + 4(\mathbf{v}_j \cdot \mathbf{v}_1) + \frac{3}{2r_j^2}(\mathbf{x}_j^h \cdot \mathbf{v}_1)^2 + \frac{5Gm_j}{r_j} + \frac{4Gm_1}{r_j} \right] \mathbf{x}_j^h \right. \\ & \left. + \frac{Gm_1}{r_j^3} [\mathbf{x}_j^h \cdot (4\mathbf{v}_j - 3\mathbf{v}_1)] \mathbf{v}_j^h \right\}, \end{aligned} \quad (\text{A1})$$

where \mathbf{x} 's and \mathbf{v} 's are barycentric positions and velocities, the superscript h refers to heliocentric coordinates, and $r_j = |\mathbf{x}^h|$. The 1PN acceleration on the Sun is:

$$\begin{aligned} \tilde{\mathbf{a}}_1 = & \sum_{j=2}^N \frac{1}{c^2} \left\{ \frac{Gm_j}{r_j^3} \left[v_1^2 + 2v_j^2 - 4(\mathbf{v}_j \cdot \mathbf{v}_1) - \frac{3}{2r_j^2}(\mathbf{x}_j^h \cdot \mathbf{v}_j)^2 - \frac{4Gm_j}{r_j} - \frac{5Gm_1}{r_j} \right] \mathbf{x}_j^h \right. \\ & \left. + \frac{Gm_j}{r_j^3} [\mathbf{x}_j^h \cdot (4\mathbf{v}_1 - 3\mathbf{v}_j)] \mathbf{v}_j^h \right\}. \end{aligned} \quad (\text{A2})$$

As `mercury6`'s Bulirsch-Stoer algorithm uses heliocentric coordinates ($\mathbf{x}_j^h = \mathbf{x}_j - \mathbf{x}_1$), the 1PN acceleration on planet j in heliocentric coordinates is required, given by:

$$\tilde{\mathbf{a}}_j^h = \tilde{\mathbf{a}}_j - \tilde{\mathbf{a}}_1. \quad (\text{A3})$$

The above equations were implemented in the force calculation routines of `mercury6`.

Furthermore, the energy and angular momentum correction terms in the 1PN approximation are (Poisson & Will 2014):

$$\tilde{E}_j = \frac{\eta_j M_j}{c^2} \left\{ \frac{3}{8}(1 - 3\eta_j)(v_j^h)^4 + \frac{GM_j}{2r_j} \left[(3 + \eta_j)(v_j^h)^2 + \frac{\eta_j}{r_j^2}(\mathbf{x}_j^h \cdot \mathbf{v}_j^h)^2 \right] + \frac{G^2 M_j^2}{2r_j^2} \right\} \quad (\text{A4})$$

$$\tilde{\mathbf{L}}_j = \frac{\eta_j M_j}{c^2} \left[\frac{1}{2}(1 - 3\eta_j)(v_j^h)^2 + (3 + \eta_j)\frac{GM_j}{r_j} \right] \mathbf{x}_j^h \times \mathbf{v}_j^h, \quad (\text{A5})$$

where $\eta_j = m_1 m_j / M_j^2$ and $M_j = m_1 + m_j$. These correction terms were added to the routine `mxx_en()`, which computes energy and angular momentum in `mercury6`. Finally, the 1PN Solar System barycenter in the present approximation is given by (Newhall et al. 1983):

$$\mathbf{0} = m_1 \mathbf{x}_1 \left(1 + \frac{1}{2c^2} v_1^2 - \sum_{j=2}^N \frac{Gm_j}{2c^2 r_j} \right) + \sum_{j=2}^N m_j \mathbf{x}_j \left(1 + \frac{1}{2c^2} v_j^2 - \frac{Gm_1}{2c^2 r_j} \right), \quad (\text{A6})$$

which was used in the conversion between heliocentric and barycentric coordinates.

The results obtained with `mercury6` and the above GR implementation may be compared to results obtained with `HNBody` (both Bulirsch-Stoer, relative accuracy 10^{-15}). For example, over the 21st century, Mercury's average perihelion precession (only due to GR) was $0.42977'' \text{ y}^{-1}$ computed with `HNBody` and $0.42976'' \text{ y}^{-1}$ computed with `mercury6` and 1PN corrections. In terms of Mercury's eccentricity ($e_{\mathcal{M}}$) evolution, the difference in $e_{\mathcal{M}}$ between `HNBody` and `mercury6` runs (both Bulirsch-Stoer with GR correction) was $\lesssim 10^{-5}$ over 2 Myr starting at present initial conditions.

REFERENCES

- Agresti, A., & Coull, B. A. 1998, *Am. Stat.*, 52, 119
- Batygin, K., & Laughlin, G. 2008, *Astrophys. J.*, 683, 1207
- Batygin, K., Morbidelli, A., & Holman, M. J. 2015, *Astrophys. J.*, 799, 120
- Chambers, J. E. 1999, *Mon. Not. R. Astron. Soc.*, 304, 793
- Chambers, J. E., Wetherill, G. W., & Boss, A. P. 1996, *Icarus*, 119, 261
- Einstein, A. 1916, *Annalen der Physik*, VI. Folge, 49(7), 769
- Ito, T., & Tanikawa, K. 2002, *MNRAS*, 336, 483
- Laplace, P. S. 1951, in (Dover Publications, New York)
- Laskar, J. 1989, *Nature*, 338, 237
- Laskar, J. 2013, in *Progress in Mathematical Physics*, Vol. 66, *Chaos*, ed. B. Duplantier, S. Nonnenmacher, & V. Rivasseau (Springer Basel), 239–270
- Laskar, J., & Gastineau, M. 2009, *Nature*, 459, 817
- Morbidelli, A. 2002, *Modern Celestial Mechanics: Aspects of Solar System Dynamics* (Taylor & Francis, London)
- Murray, N., & Holman, M. 1999, *Science*, 283, 1877
- Newhall, X. X., Standish, E. M., & Williams, J. G. 1983, *Astron. Astrophys.*, 125, 150
- Oppenheimer, B. R., Baranec, C., Beichman, C., et al. 2013, *Astrophys. J.*, 768, 24
- Poisson, E., & Will, C. M. 2014, *Gravity: Newtonian, Post-Newtonian, Relativistic* (Cambridge, pp. 780: Cambridge University Press)
- Quinn, T. R., Tremaine, S., & Duncan, M. 1991, *Astron. J.*, 101, 2287
- Rauch, K. P., & Hamilton, D. P. 2002, in *Bull. Am. Astron. Soc.*, Vol. 34, *AAS/Division of Dynamical Astronomy Meeting #33*, 938
- Rauch, K. P., & Holman, M. 1999, *Astron. J.*, 117, 1087
- Richter, P. H. 2001, in *Reviews in Modern Astronomy: Dynamic Stability and Instabilities in the Universe*, ed. R. E. Schielicke, Vol. 14, 53–92
- Rushby, A. J., Claire, M. W., Osborn, H., & Watson, A. J. 2013, *Astrobiology*, 13, 833
- Saha, P., & Tremaine, S. 1992, *Astron. J.*, 104, 1633
- Schröder, K.-P., & Smith, R. C. 2008, *Mon. Not. R. Astron. Soc.*, 386, 155
- Soffel, M. H. 1989, *Relativity in Astrometry, Celestial Mechanics and Geodesy* (Springer-Verlag Heidelberg, pp. 208)
- Sussman, G. J., & Wisdom, J. 1992, *Science*, 257, 56
- Varadi, F., Runnegar, B., & Ghil, M. 2003, *Astrophys. J.*, 592, 620
- Wisdom, J., & Holman, M. 1991, *Astron. J.*, 102, 1528
- Zeebe, R. E. 2015, *Astrophys. J.*, 798, 8

Table 2: Initial conditions of the eight planets and Pluto^a for 5-Gyr runs from DE431. Heliocentric positions \mathbf{x} (AU) and velocities \mathbf{v} (AU day⁻¹).

	x	y	z
	Mercury		
\mathbf{x}	-1.40712354144735680E-01	-4.43906230277241465E-01	-2.33474338281349329E-02
\mathbf{v}	+2.11691765462179472E-02	-7.09701275933066148E-03	-2.52278032052283448E-03
	Venus		
\mathbf{x}	-7.18629835259113170E-01	-2.25188858612526514E-02	+4.11716131772919824E-02
\mathbf{v}	+5.13955712094533914E-04	-2.03061283748202266E-02	-3.07198741951420558E-04
	Earth + Moon		
\mathbf{x}	-1.68563248623229384E-01	+9.68761420122898564E-01	-1.15183154209270563E-06
\mathbf{v}	-1.72299715055074729E-02	-3.01349780674632205E-03	+2.41254068070491868E-08
	Mars		
\mathbf{x}	+1.39036162161402177E+00	-2.09984400533893799E-02	-3.46177919349353047E-02
\mathbf{v}	+7.47813544105227729E-04	+1.51863004086334515E-02	+2.99756038504512547E-04
	Jupiter		
\mathbf{x}	+4.00345668418424960E+00	+2.93535844833712467E+00	-1.01823217020834328E-01
\mathbf{v}	-4.56348056882991196E-03	+6.44675255807273997E-03	+7.54565159392195741E-05
	Saturn		
\mathbf{x}	+6.40855153734800886E+00	+6.56804703677062207E+00	-3.69127809402511886E-01
\mathbf{v}	-4.29112154163879215E-03	+3.89157880254167561E-03	+1.02876894772680478E-04
	Uranus		
\mathbf{x}	+1.44305195077618524E+01	-1.37356563056406209E+01	-2.38128487167790809E-01
\mathbf{v}	+2.67837949019966498E-03	+2.67244291355153403E-03	-2.47764637737944378E-05
	Neptune		
\mathbf{x}	+1.68107582839480649E+01	-2.49926499733276124E+01	+1.27271208982211476E-01
\mathbf{v}	+2.57936917068014599E-03	+1.77676956230748452E-03	-9.59089132565213410E-05
	Pluto		
\mathbf{x}	-9.87686582399026491E+00	-2.79580297772433077E+01	+5.85080284687055574E+00
\mathbf{v}	+3.02870206449818878E-03	-1.53793257901232473E-03	-7.12171623386267461E-04

^aMasses (Mercury to Pluto in solar masses): 1.66013679527193035E-07, 2.44783833966454472E-06, 3.04043264626852573E-06, 3.22715144505387430E-07, 9.54791938424322164E-04, 2.85885980666102893E-04, 4.36625166899970042E-05, 5.15138902053549668E-05, 7.40740740740710E-09.